






Article

A Low-Cost Microwave Filter with Improved Passband and Stopband Characteristics Using Stub Loaded Multiple Mode Resonator for 5G Mid-Band Applications

Falih M. Alnahwi ¹, Yasir I. A. Al-Yasir ^{2,*}, Abdulghafor A. Abdulhameed ³, Abdulkareem S. Abdullah ¹ and Raed A. Abd-Alhameed ²

- ¹ Department of Electrical Engineering, College of Engineering, University of Basrah, Basrah 61001, Iraq; fma3nc@mail.missouri.edu (F.M.A.); drasabdallah@ieee.org (A.S.A.)
- ² Faculty of Engineering and Informatics, University of Bradford, Bradford BD7 1DP, UK; r.a.abd@bradford.ac.uk
- ³ Department of Applied Electronics and Telecommunication, Faculty of Electrical Engineering, University of West Bohemia, 301 00 Plzeň 3, Czech Republic; abdalhme@fel.zcu.cz
- * Correspondence: y.i.a.al-yasir@bradford.ac.uk; Tel.: +44-127-423-8047

Abstract: This paper presents the design and implementation of a printed circuit microwave band-pass filter for 5G mid-band applications, using a Stub Loaded Multiple Mode Resonator (SL-MMR) technique. The objective of this article is to introduce a low-cost microstrip filter with improved passband and stopband characteristics, based on a mathematical analysis of stub loaded resonators. The filter cost is reduced by selecting the low-cost FR4 dielectric material as a substrate for the proposed filter. Based on the transmission line model of the filter, mathematical expressions are derived to predict the odd-mode and the even-mode resonant frequencies of the SL-MMR. The mathematical model also highlights the capability of controlling the position of the SL-MMR resonant frequencies, so that the 5G sub-band that extends along the range (3.7–4.2 GHz) can perfectly be covered with almost a flat passband. At the resonance frequency, a fractional bandwidth of 12.8% (500 MHz impedance bandwidth) has been obtained with a return loss of more than 18 dB and an insertion loss of less than 2.5 dB over the targeted bandwidth. Furthermore, a pair of parasitic elements is attached to the proposed filter to create an additional transmission zero in the lower stopband of the filter to enhance the suppression of the filter stopband. The measured and simulation results are well agreed, and both reveal the acceptable performance of the stopband and passband characteristics of the filter.

Keywords: microwave; 5G; Stub Loaded Multiple Mode Resonator; filter; FR4



Citation: Alnahwi, F.M.; Al-Yasir, Y.I.A.; Abdulhameed, A.A.; Abdullah, A.S.; Abd-Alhameed, R.A. A Low-Cost Microwave Filter with Improved Passband and Stopband Characteristics Using Stub Loaded Multiple Mode Resonator for 5G Mid-Band Applications. *Electronics* **2021**, *10*, 450. <https://doi.org/10.3390/electronics10040450>

Academic Editor:

Hirokazu Kobayashi

Received: 1 January 2021

Accepted: 6 February 2021

Published: 11 February 2021

Publisher's Note: MDPI stays neutral with regard to jurisdictional claims in published maps and institutional affiliations.



Copyright: © 2021 by the authors. Licensee MDPI, Basel, Switzerland. This article is an open access article distributed under the terms and conditions of the Creative Commons Attribution (CC BY) license (<https://creativecommons.org/licenses/by/4.0/>).

1. Introduction

The deployment of wireless communication applications has motivated consumers to demand modern communication with a high transmission speed [1]. Nowadays, the development of wireless communications has promoted mobile communications technology to reach its Fifth Generation (5G) [2,3]. The 5G NR bands n77 (3300–4200 MHz), n78 (3300–3800 MHz) and n79 (4400–5000 MHz) have been planned for the 5G network [4,5]. Within this wide range spectrum, 5G applications do not require the entire sub-6 GHz bandwidth, although the required channel bandwidths for 5G systems could be 5–400 MHz [6–8]. For very high data rate transmission, the researchers also suggest the millimeter waves (mmWaves) as a vacant spectrum that can entirely be utilized for the 5G applications. However, the spectrum that is extended along the frequency band (2–8 GHz) is divided into a number of sub-bands to form the 5G 6 GHz sub-band (mid-band) communications, in order to be compatible with the already existing 4G devices [9,10]. The 6 GHz sub-bands used in the US are the (3.1–3.55 GHz) and (3.7–4.2 GHz) bands. Since the 6 GHz sub-bands

are intervened with the congested wireless spectrum, it is important to insert microwave filters with improved passband and stopband characteristics to avoid interfering with the adjacent wireless applications [11].

Many researchers have proposed the Multiple Mode Resonators (MMR) to be the basis in the design of compact microwave bandpass filters (BPF) [12–22]. The MMR was used to generate a multi-band band-pass filtering response [12], and the slot line version of the MMR was utilized to design a differential mode BPF [13]. The MMR was attached by a quarter wavelength resonator to provide electric and magnetic coupling in order to generate multiple passbands [14]. The position of the filter passband was tuned with the aid of varactor diodes [15]. The square ring resonator was suggested as an MMR, and the mathematical model of the proposed design was presented to give an accurate prediction for the resonance of the MMR [16]. The cavity resonator was used as an MMR to control the transmission zeros of a BPF [17]. A combination of MMRs was devoted to design a sept-band BPF [18]. The MMR was attached to antennas to provide a stopband antenna radiation [19] or sharp bandpass radiation [20,21].

In [23], a dual-band bandpass filter using a quad-mode resonator was designed using a stub-loaded quad-mode resonator technique. Every two modes of operation, which can be flexibly adjusted, were employed to design a passband with a high degree of freedom to control the s-parameter characteristics. Source-load coupling technique and hook-shaped transmission lines were utilized to enhance the performance of the filter. Moreover, a microstrip BPF with a stub-to-stub coupling configuration to split two identical odd-modes was presented in [24]. As part of this, these two coupling stubs are folded inward to generate extra transmission zeros, which separates four modes into two parts corresponding to two passbands. The first passband is introduced by even-mode analysis, and the second passband is presented by odd-mode excitations. The operating frequency and the impedance bandwidth of each passband were adjusted by setting out the coupling coefficients and the transmission line configuration.

In [25], a design of a closed-loop rectangular BPF was proposed to operate at L1 and L2 global positioning system (GPS) applications. The design was formed by coupled-line ring resonators, a pair of open stub lines and two 0-degree parallel-coupled transmission lines. The proposed ring resonators have a symmetrical configuration, therefore, the even-/odd-mode analysis was utilized to study and derive its equivalent circuits. The filter was implemented on FR-4 dielectric material with a permittivity of 3.5 and a thickness of 1.5 mm. In this design, two passbands with a -10 dB return loss were obtained. The low passband is located at 1.3 GHz, and can be applied for the L2 GPS systems, while the high passband is centered at 1.6 GHz for use in L1 GPS systems, with an insertion loss of more than 20 dB.

A compact multiband BPF with improved bandpass and stopband characteristics and a quad cross-stub stepped impedance resonator (QC-SSIR) was introduced in [26]. A crossed-open-stub resonator structure and the ABCD matrix were used to analyze and discuss the presented filter. The microstrip design was implemented on an FR4 substrate with $\epsilon_r = 4.4$, thickness $h = 1.6$ mm and tangent loss of 0.0265. In addition, a folded stepped impedance resonator technique was employed to reduce the filter size by up to 46% compared with the other presented designs. The presented filter using a new configuration has achieved transmission coefficients/fractional bandwidths of 0.60 dB/49.3%, 1.49 dB/18.7% and 1.93 dB/ 13.9% at 0.81 GHz, 1.71 GHz and 2.58 GHz, respectively.

Other technologies such as low-temperature co-fired ceramic (LTCC), high-temperature co-fired ceramic (HTCC), high-temperature superconductors (HTS), integrated passive device (IPD) and reconfigurable/tunable and acoustic structures can also be deployed for the 5G systems [27–37]. Some of these techniques aim to reduce the overall size of the BPF components, and obtain good filtering performance [27–30]. While the size of the system can be reduced, the filters designed by these processes still have poor roll-off and relatively high insertion losses. In contrast, the IPD technologies based on substrates such as silicon,

GaAs (Gallium Arsenide) and glass can deliver better properties for microwave devices in current and future 5G wireless communication systems [27,28].

On the other hand, the planar lumped element filters can be designed as microwave integrated circuits (MICs), monolithic microwave integrated circuits (MMICs), low temperature co-fired ceramics (LTCC), and also in high-temperature superconductors (HTS). Generally, planar lumped element filter designs are restricted by a lower quality factor and lower power handling, as compared with the bulkier lumped element structures [29,30]. The LTCC-based components are a mechanically strong, hermetic, chemically inert and dimensionally stable ceramic structure with very stable dielectric properties [30]. While the cost of LTCC materials is considerably high in comparison to the circuits implemented by FR4-printed circuit boards, their price is anticipated to be more or less the same in nearest future. In [29], an LTCC BPF structure is designed based on the S–L coupling, where high selectivity and a wide stopband have been obtained, which made the designed filter suitable for system-in-package (SiP) platforms.

Moreover, state-of-the-art acoustic filters based on lithium tantalite (LiTaO₃) or lithium niobate (LiNbO₃) surface acoustic wave (SAW) resonators and aluminum nitride (AlN) bulk acoustic wave (FBAW) resonators can be challenging to support the emerging 5G new radio (NR) requiring more than 5% FBW without resorting to lumped-element-based bandwidth widening techniques [31,32]. Furthermore, hybrid filter design techniques, using the combination of IPD and acoustic topologies, are proposed to satisfy the new demands in 5G NR systems, where high frequency and wide bandwidth are required by these standardizations [34,35]. These methodologies will employ both lumped-LC IPD structures and high-quality factor acoustic resonators.

In this work, a low-cost planar microwave BPF with improved filter characteristics is presented for 5G sub-6 GHz band occupying the range (3.7–4.2 GHz). The FR4 dielectric material is selected to be the dielectric substrate of the proposed filter for cost reduction purposes. The structure of the filter consists of a Stub Loaded Multiple Mode Resonator (SL-MMR), which is coupled with the feed line through the parallel line coupling technique. With the aid of the transmission line model of the filter, two expressions are developed to estimate the position of the odd-mode resonant frequency and the even mode resonant frequency. The positions of the resonant frequencies are modified until obtaining almost a flat passband response, along with the aforementioned band of interest. Moreover, the stopband suppression is improved by attaching a pair of parasitic elements to produce an additional transmission zero at the lower stopband. The measured and simulation results are in good congruence, and they successfully verify the acceptable performance of the proposed filter despite its reduced cost.

2. Filter Structure

The proposed filter consists of a Stub Loaded Multiple Mode Resonator (SL-MMR) that provides almost a flat passband and a pair of parasitic elements for stopband suppression improvement. Figure 1a illustrates the structure and the positions of the SL-MMR and the parasitic elements, as well as the dimensions of their components. The SL-MMR is inserted between two 50 Ω microstrip feed lines, and it is coupled to them via a parallel line coupling, whose dimensions are shown in Figure 1b. The dielectric substrate that is used for this design is the low cost FR4 dielectric material with dielectric constant $\epsilon_r = 4.3$, loss tangent of 0.025 and height $h = 1.6$ mm. It is well known that the backside of the dielectric material is fully covered with a metallic ground plane.

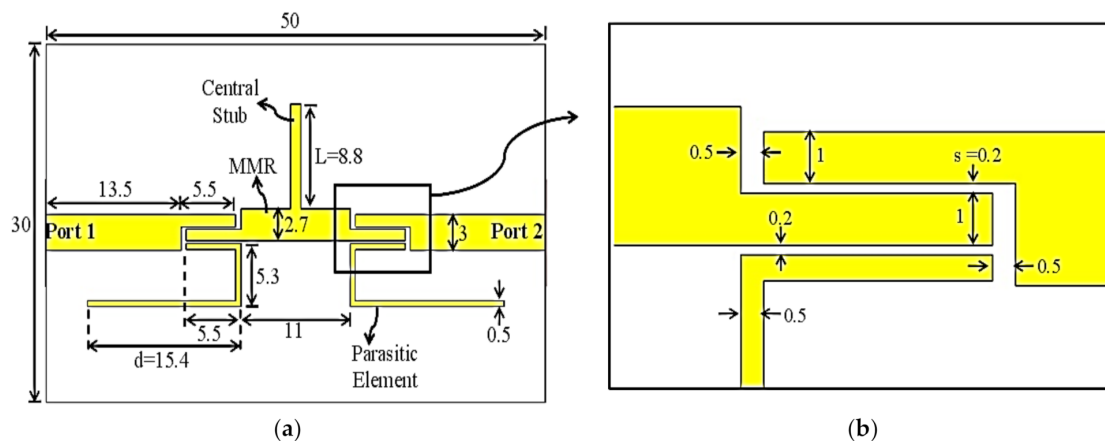


Figure 1. Geometry of the proposed filter: (a) dimensions of the overall structure and; (b) dimensions of the parallel line coupler (all dimensions are in mm).

3. Filter Analysis and Modeling

Before delving into the transmission line model of the SL-MMR and the parasitic elements, some basic equations should be recalled to make the filter analysis more understandable. The microstrip line characteristic impedance (Z_0) and the effective dielectric constant (ϵ_{re}) can be evaluated from the empirical equations given in [38]. In addition, the input impedance (Z_{in}) of a lossless transmission line whose characteristic impedance Z_0 and terminated by a load impedance Z_L is given in [39].

Based on the quasi-TEM behavior of the microstrip line, the phase constant (β) can be related to the transmission line resonant frequency using the following formula [39]

$$\beta = 2\pi f_r \frac{\sqrt{\epsilon_{re}}}{c} \quad (1)$$

where f_r represents the resonant frequency, and c denotes the speed of light in the free space. With the aid of the aforementioned equations, the mathematical estimation of the resonant frequencies of the SL-MMR and the parasitic elements can be presented as given in the following two sub-sections.

3.1. SL-MMR Modeling

In fact, the SL-MMR has a symmetrical structure with respect to the vertical axis shown in Figure 2a. Thereby, the even and odd modes kind of analysis is the best way that can be followed to estimate the resonant frequencies of the proposed SL-MMR, as demonstrated in the below sub-sections. It is worth mentioning that the resonant frequencies of the odd and even modes are found by presenting a weak coupling between the feed line and the SL-MMR [40,41]. In this work, the week coupling is produced by setting the feed arm length (shown in Figure 2a) to 1.5 mm, and is then set back to 5.5 mm for the rest of the simulation process. The simulation process was performed using CST Microwave Studio Simulation Suite.

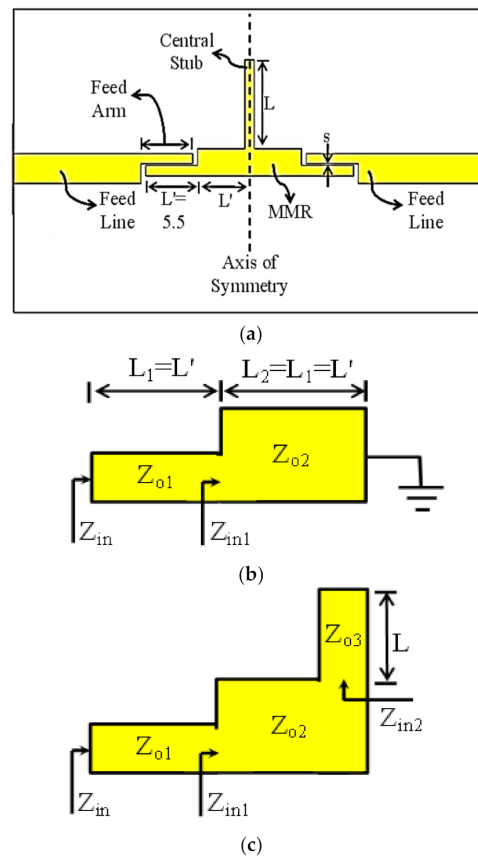


Figure 2. The structure of the proposed Stub Loaded Multiple Mode Resonator (SL-MMR): (a) the entire SL-MMR; (b) odd mode; and (c) even mode (all dimensions are in mm).

3.1.1. Odd-Mode Resonant Frequency

The odd mode is obtained by exciting the filter ports with two different sources whose signals are equal in amplitude and 180° out of phase. In this case, the voltage signals at the axis of symmetry have equal amplitudes but with 180° phase shift, while the current signals have equal amplitude with zero phase shift. Consequently, at the resonant frequency, the resulted voltage at the axis of symmetry is equal to zero, while the current signal is at its maximum value which is equivalent to the short circuit case. Because of this short circuit, the effect of the central stub is canceled, as shown in Figure 2b. Consider that Z_{o1} and Z_{o2} are the characteristic impedances of the first and second pieces of the odd-mode SL-MMR, respectively. On the other hand, Z_{in} and Z_{in1} are the input impedance and the input impedance seen at the input of the second piece of the odd-made SL-MMR, respectively. In addition, L_1 and L_2 are the lengths of the first and second pieces of odd-mode SL-MMR, respectively. For simplicity, the two lengths are set to be equal ($L_1 = L_2 = L'$). Applying input impedance equation with $Z_L = 0$ results in:

$$Z_{in1} = jZ_{o2}\tan(\beta L') \tag{2}$$

It should be noted that β is approximated to be the phase constant of the feed line [42,43]. Therefore, the input impedance of the odd-mode structure is given by:

$$Z_{in} = Z_{o1} \frac{Z_{in1} + jZ_{o1} \tan(\beta L')}{Z_{o1} + jZ_{in1} \tan(\beta L')} \tag{3}$$

The condition of resonance is that the input impedance should equal infinity $Z_{in} = \infty$ at the resonant frequency [41]. Thus,

$$Z_{o1} + jZ_{in1} \tan(\beta L') = 0 \quad (4)$$

After substituting the value of Z_{in1} given in (2), then:

$$\beta L' = \tan^{-1} \left(\sqrt{\frac{Z_{o1}}{Z_{o2}}} \right) \quad (5)$$

By combining (5) and (1), the odd-mode resonant frequency (f_{ro}) can be obtained as follows

$$f_{ro} = \frac{c}{2\pi L' \sqrt{\epsilon_{re}}} \tan^{-1} \left(\sqrt{\frac{Z_{o1}}{Z_{o2}}} \right) \quad (6)$$

where ϵ_{re} is the effective dielectric constant of the feed line.

3.1.2. Even-Mode Resonant Frequency

The even mode is achieved by exciting the ports of the filter with two identical signals (equal amplitudes and phase angles). At the axis of symmetry, the voltage signals are with equal amplitude and phase angles, while the current signals are with equal amplitude and 180 out of phase. Thereby, a maximum voltage value is appeared at the axis of symmetry and zero current value at the resonant frequency, and this is equivalent to the open circuit. In this case, the effect of the central stub appears as shown in Figure 2c, and the axis of symmetry cuts the central stub into two halves. Let Z_{o3} be the characteristic impedance of one half of the stub, and Z_{in2} be the input impedance of the half of the stub. Since the stub is terminated by an open circuit ($Z_L = \infty$), the value of Z_{in2} can be calculated as follows

$$Z_{in2} = -jZ_{o3} \cot(\beta L) \quad (7)$$

where L is the length of the stub. Similarly:

$$Z_{in1} = Z_{o2} \frac{Z_{in2} + jZ_{o2} \tan(\beta L')}{Z_{o2} + jZ_{in2} \tan(\beta L')} \quad (8)$$

$$Z_{in} = Z_{o1} \frac{Z_{in1} + jZ_{o1} \tan(\beta L')}{Z_{o1} + jZ_{in1} \tan(\beta L')} \quad (9)$$

As mentioned earlier, at the resonant frequency, the input impedance is equal to infinity ($Z_{in} = \infty$). As a result, the denominator of (9) should equal zero:

$$Z_{o1} + jZ_{in1} \tan(\beta L') = 0 \quad (10)$$

By substituting (7) and (8) into (10), the resonance formula is modified as follows:

$$\cot(\beta L) = \frac{Z_{o2}}{Z_{o3}(Z_{o1} + Z_{o2})} [Z_{o2} \tan(\beta L') - Z_{o1} \cot(\beta L')] \quad (11)$$

By using (1) and with the aid of a simple computer program code, the even resonant frequency (f_{re}) can be predicted.

To verify the accuracy of the proposed mathematical models, the mathematically estimated values of the odd-mode and even-mode resonant frequencies are compared with those resulting from CST Microwave Studio. Figure 3a illustrates the estimated and simulated odd-mode resonant frequencies for different MMR parts length (L'), while Figure 3b shows the estimated and simulated even-mode resonant frequencies for different stub length values (L) and $L' = 5.5$ mm. It is clear that the proposed mathematical expressions give a very reasonable prediction about the resonant frequencies of the SL-

MMR. The discrimination between the estimated and simulated results comes from many reasons, such as the mathematical equations assuming lossless transmission lines, empirical equations of Z_0 and ϵ_{re} are not perfect, and β is approximated to be the phase constant of the feed line, as mentioned earlier in this sub-section. However, considering the aforesaid assumptions drastically complicates the mathematical model of the proposed SL-MMR, with a small improvement in the deviation of the curves.

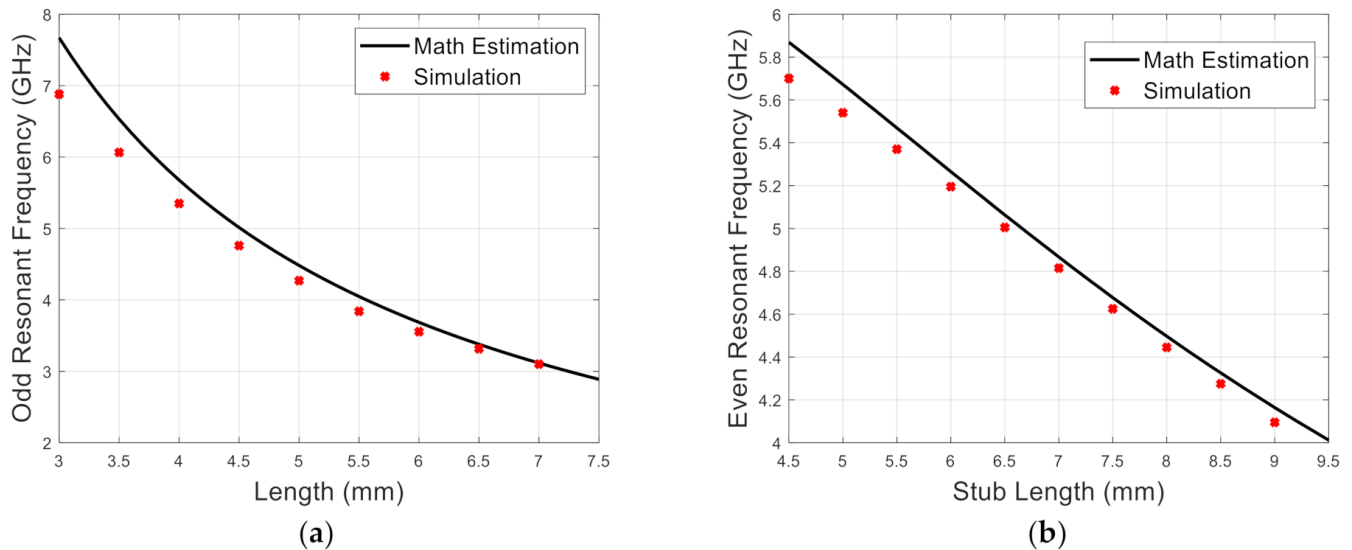


Figure 3. A comparison between the SL-MMR estimated and the CST Microwave Studio simulated resonant frequencies for: (a) odd mode (variable L'); and (b) even mode (variable L).

To fortify the approximation of the odd-mode and even-mode analysis, Figure 4 demonstrates the current distribution of the SL-MMR at the odd-mode resonant frequency (3.87 GHz) and the even-mode resonant frequency (4.1 GHz) for $L' = 5.5$ mm and $L = 8.8$ mm. At the odd mode, the current is negligible at and around the central stub as shown in Figure 4a. This result supports the hypothesis of the odd mode, which states that the central stub does not contribute to determining the resonant frequency of the odd mode. Nevertheless, Figure 4b reveals that the current is dense at the central stub when the even mode is applied.

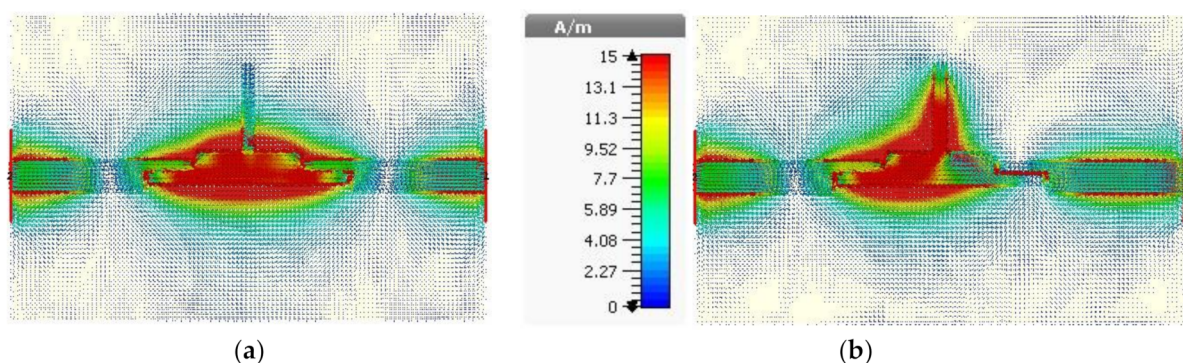


Figure 4. The current distribution of the SL-MMR at $L = 8.8$ mm and $L' = 5.5$ mm: (a) odd mode ($f = 3.87$ GHz) and (b) even mode ($f = 4.1$ GHz).

3.2. Parasitic Elements Modeling

As will be discussed in the next section, the parallel line coupling introduces a transmission zero at the higher stopband of the transmission coefficient of BPF. However, the

transmission coefficient of the filter has a bad suppression at the lower stopband. Therefore, a pair of parasitic elements is attached to the proposed SL-MMR (as shown in Figure 5) to generate a band notch operating as a transmission zero in order to improve the suppression of the lower stopband of the filter. Similarly, each parasitic element is treated as a piece of a microstrip transmission line with character impedance (Z_0), but it is terminated by an open circuit ($Z_L = \infty$). Consequently, the input impedance (Z_{in}) of the parasitic element is given below

$$Z_{in} = -jZ_0 \cot(\beta L_t) \quad (12)$$

where L_t is the total length of the parasitic element. Recall that the input impedance should be equal to infinity at the resonant frequency of the parasitic element, such that $\cot(\beta L_t) = \infty$. The first angle that satisfies this condition is when ($\beta L_t = \pi$). Thus, after substituting (1) into this condition, the well-known half-wavelength resonant frequency (f_r) equation is produced.

$$f_r = \frac{c}{2L_t \sqrt{\epsilon_{re}}} \quad (13)$$

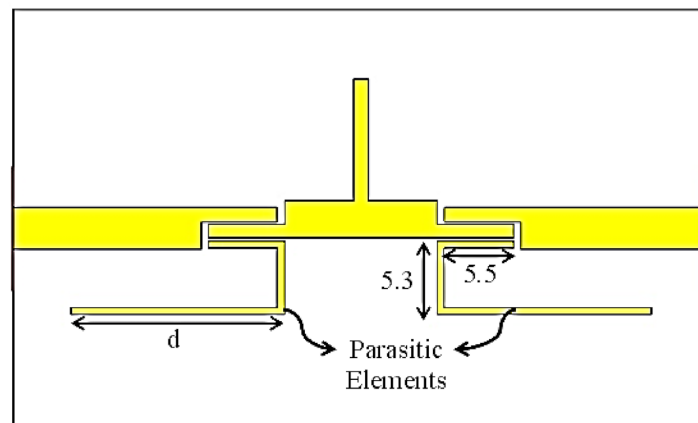


Figure 5. The parasitic elements of the proposed filter.

The above equation is tested and analyzed in most of the researches related to the band notch generation [44]. Consequently, the test of the accuracy of this equation holds only the optimum value which is obtained when the parasitic element arm (d) is equal to (51.4 mm). The overall length under this condition is found to be (26.2 mm). For this total parasitic element length, the mathematically estimated transmission zero is located at (3.18 GHz), while for the CST Microwave Studio value is (3.24 GHz).

The current distribution of the proposed BPF outside the transmission zero ($f = 3.9$ GHz) and inside it ($f = 3.24$ GHz) is illustrated in Figure 6. It is clear that the current is concentrated around the parasitic element at the transmission zero frequency $f = 3.24$ GHz, and there is a very negligible amount of current that reaches the output port (right-hand port in Figure 6a). On the other hand, the output port (right-hand port) in Figure 6b has a significant amount of current that verifies the successful energy transmission outside the transmission zero.

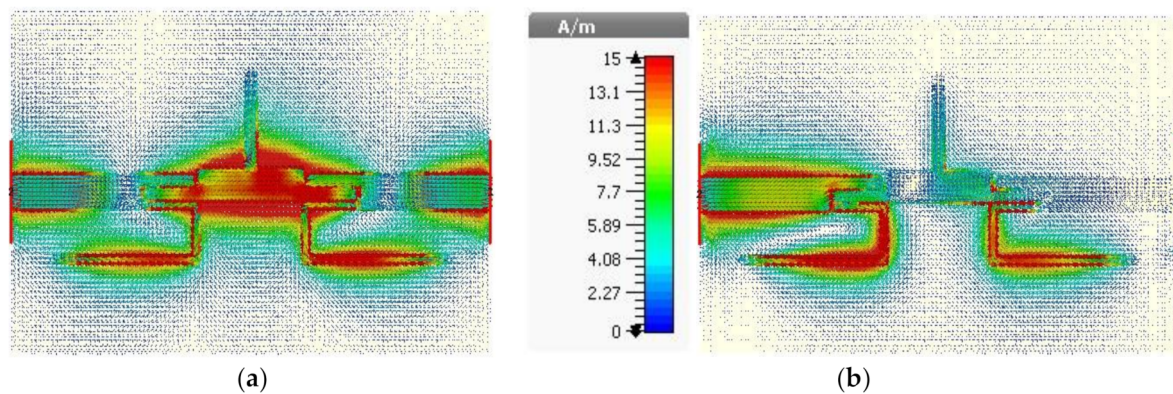


Figure 6. The current distribution of the proposed filter: (a) outside the transmission zero ($f = 3.9$ GHz); and (b) at the created transmission zero ($f = 3.24$ GHz).

4. Parametric Study

At first, the parametric study focuses on the SL-MMR without attaching the parasitic elements. Figure 7 illustrates the reflection and transmission coefficients of the SL-MMR for different parallel line coupling separation (denoted by s in Figure 2a). The smaller the separation between the parallel lines, the higher is the coupling between them, which results in a significant improvement in the BPF bandwidth. Therefore, separation $s = 0.2$ mm is the more suitable value that results in covering the intended frequency range (3.7–4.2 GHz), in addition to the almost flat transmission coefficient within the filter passband.

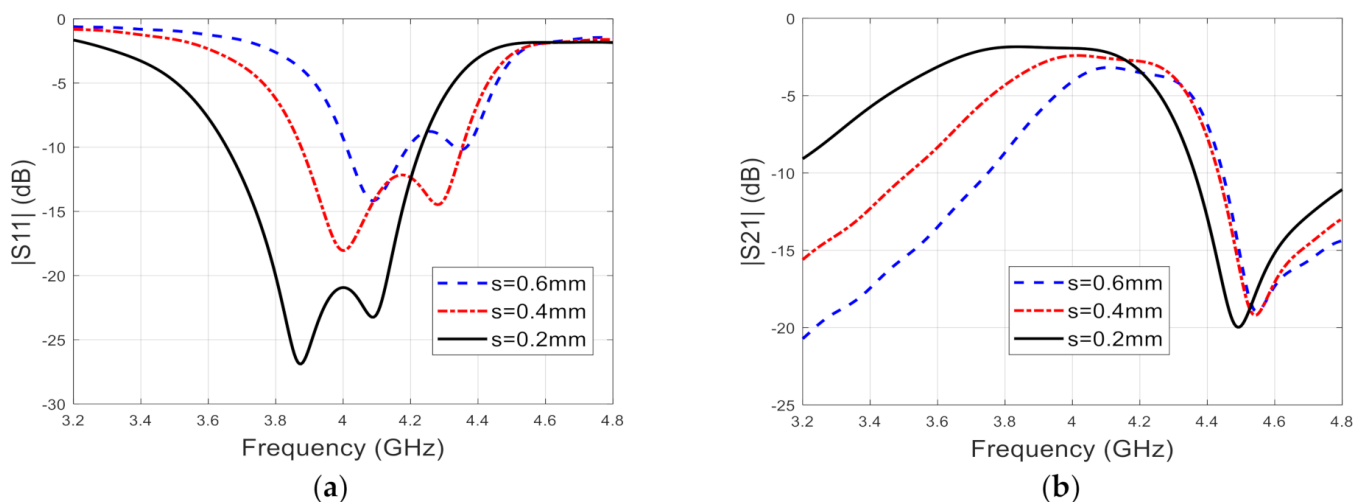


Figure 7. Simulated scattering parameters of the proposed SL-MMR-based microwave filter without the parasitic elements at $L = 8.8$ mm and different values of parallel lines separation: (a) reflection coefficient; and (b) the transmission coefficient.

The effect of the central stub of the SL-MMR is demonstrated in Figure 8. Increasing the length of the central stub (denoted by L in Figure 2a) leads to reduce the even-mode resonant frequency (the second resonant frequency) without a significant variation in the odd-mode resonant frequency. The length $L = 8.8$ mm is the value that provides very good matching within the required frequency range. Furthermore, the flatness of the transmission coefficient at the passband is guaranteed at this value of stub length. Figure 8 also accentuates two different modes of operation for the proposed filter:

- a. The dual narrowband mode can be obtained when a short central stub (or no central stub) is attached to the filter. This design is beneficial for only specific applications within this 5G sub-band, but with an improved quality factor.

- b. The second mode (the main concern of this work) is obtained when a longer central stub is used. In this case, the even and odd resonant frequencies are getting closer to each other to cover wider bandwidth. The advantage of this mode is concluded by covering the entire 5G sub-band with good matching characteristics to make the device, to which the filter is attached, compatible with the entire band of interest.

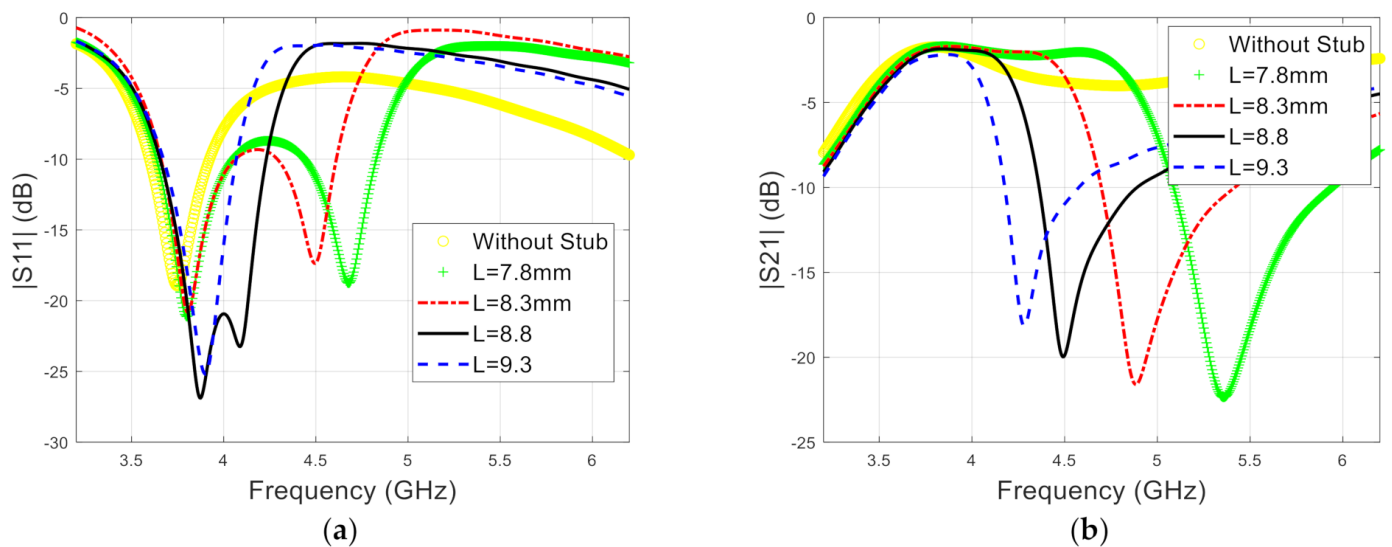


Figure 8. Simulated scattering parameters of the proposed SL-MMR based microwave filter without the parasitic elements at $s = 0.2$ mm and different values stub length: (a) reflection coefficient; and (b) the transmission coefficient.

It can be seen that the parallel line coupling provides a transmission zero at the upper stopband of the proposed BPF. However, the transmission coefficient at the lower stopband has relatively high values, so the parasitic elements are inserted to present a band notch at the lower stopband. Figure 9 illustrates the effect of the parasitic element on the scattering parameters of the proposed BPF. Increasing the length of the parasitic element arm length (denoted by d in Figure 5) decreases the position of the transmission zero in the transmission coefficient curve. The value of the parasitic element arm $d = 15.4$ mm results in an overall parasitic element length equal to (26.2 mm). This value leads to set the transmission zero position at 3.24 GHz, with a minor effect on the reflection and transmission coefficients within the filter passband.

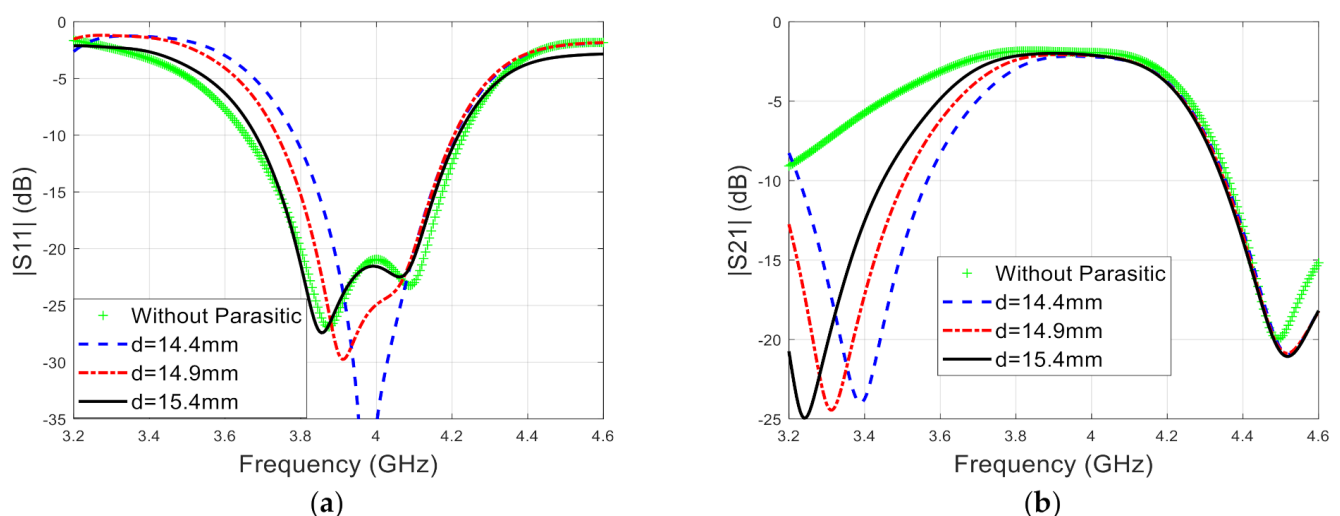


Figure 9. Simulated scattering parameters of the proposed SL-MMR based microwave filter with the parasitic elements at different values of parasitic element arm length d : (a) reflection coefficient; and (b) the transmission coefficient.

5. Measured Results

Figure 10 shows a photograph of the prototype of the proposed filter. The measurements are acquired using an AMITEC network analyzer, and the filter substrate is made of low-cost FR4 dielectric material. The measured reflection and transmission coefficients are compared with their simulated equivalent in Figure 11. The simulated reflection coefficient reveals a very satisfactory matching within the passband, and also shows a filter bandwidth extended along with the range (3.67–4.22 GHz), while the measured bandwidth occupies the range (3.71–4.2 GHz). On the other hand, the measured and simulated transmission coefficients are also well agreed, where both show almost a flat response within the passband, which is surrounded by two transmission zeros. The simulation transmission zeros are located at 3.24 GHz and 4.52 GHz, while the measured transmission zeros are at 3.31 GHz and 4.45 GHz. With the presence of these two transmission zeros, the filter suppression for the adjacent band signals is noticeably improved.



Figure 10. The prototype of the proposed microwave filter.

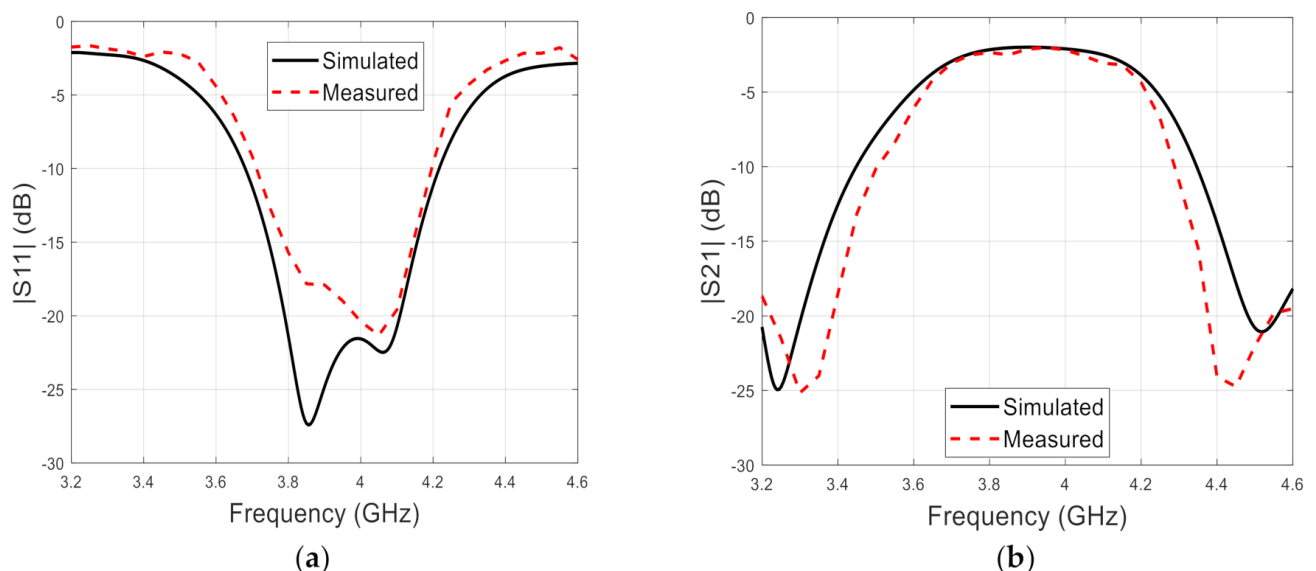


Figure 11. Measured versus simulation scattering parameters of the proposed microwave filter: (a) reflection coefficient; and (b) transmission coefficient.

The deviation between the simulated and measured results may be attributed to many reasons, such as the imperfect engraving of the laser cutting CNC machine (LPKF ProtoMat S42) used in this work and the imperfect soldering of the SMA connectors. Nevertheless, the proposed filter is highly eligible for the 5G 6 GHz sub-band extended along with the range (3.7–4.2 GHz), which is used in US 5G applications. The proposed filter is

suitable for 5G portable devices to filter out the undesired frequencies before the frequency down-conversion process. Table 1 summarises the obtained simulated and measured performance, where good agreement was observed between them. Although it is easy to obtain a very high filter quality factor using cavity or cap filters, they are not compatible with portable devices that require low profile structures. The microstrip filters can easily be embedded in these kinds of devices due to their planar structure and lightweights, despite their low value of the quality factor. Moreover, Table 2 compares this proposed SIR/SLR filter with other designs, with similar configurations and performances. Figure 12 illustrates a wide-band window of the simulated and measured results. As expected, the simulated results reveal that the frequency domain characteristics have almost periodic behavior, due to the use of distributed element structure [38,39] in which the resonant properties appear at higher-order even and odd resonant frequencies. Unfortunately, the measured results could not be obtained for frequencies above 4.6 GHz due to the limited bandwidth of the network analyzer. Additionally, Figure 13 demonstrates the setup of the measurement process of the proposed filter. For future works, the designed filter can be developed as follows.

Table 1. Simulation and measurement result comparison.

Results	RL(dB) @ f_0 (GHz)	−10 dB Impedance Bandwidth (MHz)	IL(dB) @ f(GHz)	Rejection(dB) @ f(GHz)	
				Lower Band	Upper Band
Simulated	22 @ 3.95	550	21 @ 3.2 3.0 @ 3.7 2.3 @ 3.95 (f_0) 4.0 @ 4.2 17.7 @ 4.6	15 @ 3.0 21 @ 3.2 25 @ 3.24 (f_{TZs}) 14 @ 3.4	17.5 @ 5.0 14.6 @ 4.4 22 @ 4.52 (f_{TZs}) 18 @ 4.6
Measured	19 @ 3.95	490	18.4 @ 3.2 3.1 @ 3.7 2.4 @ 3.95 (f_0) 4.2 @ 4.2 19.5 @ 4.6	17 @ 3.0 18.4 @ 3.2 25 @ 3.31 (f_{TZs}) 20 @ 3.4	− @ 5.0 23 @ 4.4 24.9 @ 4.45 (f_{TZs}) 19.5 @ 4.6

f_0 : center frequency; IL: insertion loss; RL: return loss; TZs: transmission zeros.

Table 2. Comparison between the proposed design and others.

Ref.	Technique	Freq. (GHz)	−10 dB FBW (%)	RL (dB)	IL (dB)	Via Holes	Size (mm ²)
[16]	MMSRR	3.5	5.7	27	1.7	0	45 × 45
[17]	MMSIW	2.2	5.4	12	3.3	SIW	89 × 36
[18]	MMR	2.8/3.5/4.2	6.8/9.4/3.0	13/17/12	1.2/1.0/1.9	5	40 × 65
[23]	SLR	1.8/3.5	14/10	24/18	0.8/0.9	1	25 × 25
[26]	FQC-SSIR	0.8/1.8/2.62	25/10/7	15/10/14	-	0	97 × 129
[27]	IPD	3.75	24	>10	1.52	IPD	2.0 × 1.25
[29]	LTCC	2.45	10.8	>15	2.5	0	2.48 × 2.02
[30]	HTCC	2.25	5.5	>17	1.8	0	7.0 × 4.8
[31]	Acoustic Wave Hybrid	4.5	8.5	>14	2.7	0	0.64 × 1.4
[34]	(IPD & Acoustic)	3.8	22	-	2.5	IPD	2.0 × 1.8
Prop.	SIR/SLR	3.95	14	19	2.4	0	25 × 50

MMSRR: multi-mode square ring resonator; MMSIW: multi-mode square ring resonator: substrate-integrated-waveguide; SLR: stub-loaded resonator; FQC-SSIR: folded quad cross-stub stepped impedance resonator.

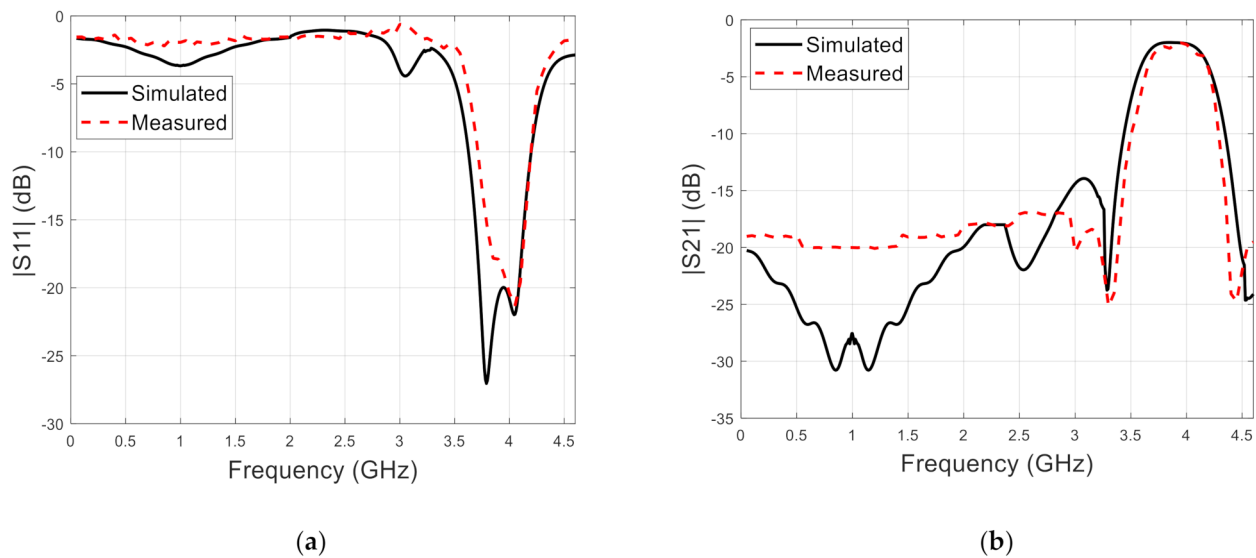


Figure 12. A wide window of the measured versus simulation scattering parameters of the proposed microwave filter: (a) reflection coefficient; and (b) transmission coefficient.

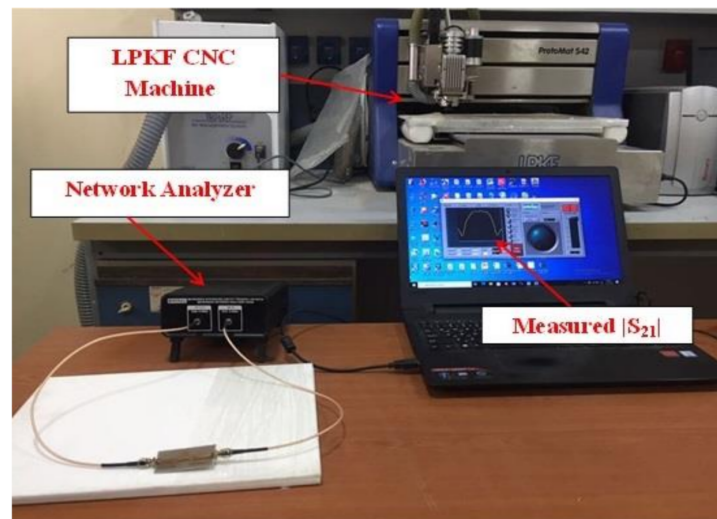


Figure 13. Photograph of the measurement setup for the proposed filter.

- Shielding the fabricated filter to provide a noticeable immunity against the electromagnetic interference;
- Controlling the electrical length of the central stub with the aid of varactor or PIN diode to present a controllable even mode resonant frequency, so that the filter can be used as a wideband 5G filter and dual-band narrow band filter.

6. Conclusions

A low-cost planar BPF for 5G 6 GHz sub-band applications has successfully been designed and fabricated. Based on the SL-MMR and with the aid of the proposed mathematical model, the bandwidth of the filter is modified to cover the intended range (3.7–4.2 GHz). Although the parallel line coupling of the SL-MMR creates a transmission zero at the upper stopband of the BPF at 4.52 GHz, the lower stopband has a weak rejection for the undesired signals. Therefore, a pair of parasitic elements is attached to the proposed BPF to present a transmission zero in the lower stopband at 3.24 GHz. It was also found that the passband of the filter has low values of reflection coefficient, with an almost flat transmission coefficient.

Author Contributions: Conceptualisation, F.M.A. and Y.I.A.A.-Y.; methodology, F.M.A.; investigation, F.M.A., Y.I.A.A.-Y., A.A.A., A.S.A. and R.A.A.-A.; resources, F.M.A. and Y.I.A.A.-Y.; writing—original draft preparation, F.M.A., Y.I.A.A.-Y., A.A.A. and A.S.A.; writing—review and editing, F.M.A., Y.I.A.A.-Y., A.A.A., A.S.A. and R.A.A.-A.; visualisation, F.M.A., Y.I.A.A.-Y., A.A.A., A.S.A. and R.A.A.-A. All authors have read and agreed to the published version of the manuscript.

Funding: This research received no external funding.

Acknowledgments: The authors wish to express their thanks for the support provided by the innovation programme under grant agreement H2020-MSCA-ITN-2016 SECRET-722424.

Conflicts of Interest: The authors declare no conflict of interest.

References

1. Mahon, S. The 5G Effect on RF Filter Technologies. *IEEE Trans. Semicond. Manuf.* **2017**, *30*, 494–499. [CrossRef]
2. Shin, K.R.; Eilert, K. Compact low cost 5G NR n78 band pass filter with silicon IPD technology. In Proceedings of the 2018 IEEE 19th Wireless and Microwave Technology Conference (WAMICON), Sand Key, FL, USA, 9–10 April 2018; pp. 1–3.
3. Abdurraheem, Y.; Hasanain, A.H.A.; Baha, A.S.; Parchin, N.O.; Ahmed, M.A.; Abdulkareem, S.A.; Raed, A.A. New Radiation Pattern-Reconfigurable 60-GHz Antenna for 5G Communications. *IntechOpen*. 2019. Available online: <https://www.intechopen.com/online-first/new-radiation-pattern-reconfigurable-60-ghz-antenna-for-5g-communications> (accessed on 26 September 2019).
4. Campanella, H.; Qian, Y.; Romero, C.O.; Wong, J.S.; Giner, J.; Kumar, R. Monolithic Multiband MEMS RF Front-End Module for 5G Mobile. *J. Microelectromechan. Syst.* **2021**, *30*, 72–80. [CrossRef]
5. Statement: Improving Consumer Access to Mobile Services at 3.6 GHz to 3.8 GHz. Available online: <https://www.ofcom.org.uk/consultations-and-statements/category-1/future-use-at-3.6-3.8-ghz> (accessed on 21 October 2018).
6. Watanabe, A.O.; Ali, M.; Sayeed, S.Y.B.; Tummala, R.R.; Raj, P.M. A Review of 5G Front-End Systems Package Integration. *IEEE Trans. Compon. Packag. Manuf. Technol.* **2020**. [CrossRef]
7. Ben Thomas, Q. Global 5G Rush But No Global 5G Handsets. *Microw. J.* **2019**, *62*, 98–103.
8. Caleffi, M.; Trianni, V.; Cacciapuoti, A.S. Self-Organizing Strategy Design for Heterogeneous Coexistence in the Sub-6 GHz. *IEEE Trans. Wirel. Commun.* **2018**, *17*, 7128–7143. [CrossRef]
9. Ban, Y.; Li, C.; Sim, C.; Wu, G.; Wong, K. 4G/5G Multiple Antennas for Future Multi-Mode Smartphone Applications. *IEEE Access* **2016**, *4*, 2981–2988. [CrossRef]
10. Liu, C.; Deng, Z.; Liu, X.; Luo, X. A Wideband Bandpass Filter with Broad Stopband and Ultra-Wide Reflectionless Range for 5G Applications. In Proceedings of the 2019 IEEE MTT-S International Microwave Symposium (IMS), Boston, MA, USA, 2–7 June 2019; pp. 834–837.
11. Al-Yasir, Y.I.A.; Tu, Y.; Parchin, N.O.; Abdulkhaleq, A.; Kosha, J.; Ullah, A.; Abd-Alhameed, R.; Noras, J. New Multi-standard Dual-Wideband and Quad-Wideband Asymmetric Step Impedance Resonator Filters with Wide Stop Band Restriction. *Int. J. Microw. Comput. Aided Eng.* **2019**, *29*, e21802. [CrossRef]
12. Xu, J.; Wu, W.; Wei, G. Compact Multi-Band Bandpass Filters with Mixed Electric and Magnetic Coupling Using Multiple-Mode Resonator. *IEEE Trans. Microw. Theory Tech.* **2015**, *63*, 3909–3919. [CrossRef]
13. Chen, D.; Bu, H.; Zhu, L.; Cheng, C. A Differential-Mode Wideband Bandpass Filter on Slotline Multi-Mode Resonator With Controllable Bandwidth. *IEEE Microw. Wirel. Compon. Lett.* **2015**, *25*, 28–30. [CrossRef]
14. Ai, J.; Zhang, Y.; Xu, K.; Li, D.; Fan, Y. Miniaturized Quint-Band Bandpass Filter Based on Multi-Mode Resonator and $\lambda/4$ Resonators with Mixed Electric and Magnetic Coupling. *IEEE Microw. Wirel. Compon. Lett.* **2016**, *26*, 343–345. [CrossRef]
15. Zhang, S.; Chen, Z.; Chu, Q. Compact Tunable Balanced Bandpass Filter with Novel Multi-Mode Resonator. *IEEE Microw. Wirel. Compon. Lett.* **2017**, *27*, 43–45. [CrossRef]
16. Zhang, J.; He, M.; Chen, H.; Pang, D.; Ji, L.; Zhao, X.; Zhang, X. Bandpass filters using multi-mode square ring resonators. *IET Microw. Antennas Propag.* **2018**, *12*, 1656–1665. [CrossRef]
17. Psychogiou, D.; Gomez-Garcia, R. Multi-Mode-Cavity-Resonator-Based Bandpass Filters With Multiple Levels of Transfer-Function Adaptivity. *IEEE Access* **2019**, *7*, 24759–24765. [CrossRef]
18. Bi, X.; Wang, L.; Ma, Q.; Hu, B.; Xu, Q. A Compact Sept-Band Bandpass Filter Utilising a Single Multi-Mode Resonator. *IET Microw. Antennas Propag.* **2019**, *13*, 2013–2019. [CrossRef]
19. Alnahwi, F.; Abdulhameed, A.; Swadi, H.; Abdullah, A. A Compact Wide-Slot UWB Antenna with Reconfigurable and Sharp Dual-Band Notches for Underlay Cognitive Radio Applications. *Turk. J. Electr. Eng. Comput. Sci.* **2019**, *27*, 94–105. [CrossRef]
20. Liu, N.; Chen, X.; Zhu, L.; Chen, X.; Fu, G.; Liu, Y. Low-Profile Triple-Band Microstrip Antenna Via Sharing a Single Multi-Mode Patch Resonator. *IET Microw. Antennas Propag.* **2019**, *13*, 1580–1585. [CrossRef]
21. Zheng, D.; Wu, K. Leaky-Wave Antenna Featuring Stable Radiation Based on Multi-Mode Resonator (MMR) Concept. *IEEE Trans. Antennas Propag.* **2020**, *68*, 2016–2030. [CrossRef]
22. Al-Yasir, Y.I.A.; Ojaroudi Parchin, N.; Abdulkhaleq, A.M.; Bakr, M.S.; Abd-Alhameed, R.A. A Survey of Differential-Fed Microstrip Bandpass Filters: Recent Techniques and Challenges. *Sensors* **2020**, *20*, 2356. [CrossRef]

23. Li, G.; Xiu, Y.Z. High-Selectivity Dual-Band Band pass Filter Using a Quad-Mode Resonator with Source-Load Coupling. *IEEE Microw. Wirel. Compon. Lett.* **2013**, *23*, 474–476.
24. Shou-Jia, S.; Tao, S.; Kun, D.; Bian, W.; Chang-Hong, L. Compact Microstrip Dual-Band Bandpass Filter Using a Novel Stub-Loaded Quad-Mode Resonator. *IEEE Microw. Wirel. Compon. Lett.* **2013**, *23*, 465–467.
25. Issa, H.; Wehbi, M. Tunable Bandpass Filter Using Series Connected Varactor Diodes. *IETE J. Res.* **2019**, 1–7. [[CrossRef](#)]
26. Wibisono, G.; Firmansyah, T.; Herudin, H.; Wildan, M.; Supriyanto, T.; Alaydrus, M.; Ujang, F. Multiwideband Bandpass Filter Based on Folded Quad Cross-Stub Stepped Impedance Resonator. *Int. J. Antennas Propag.* **2020**. [[CrossRef](#)]
27. Li, X.; Song, J.; Wang, D.; Qin, Q.; Sun, L. A Highly Selective and Compact 5G n77 Band Pass Filter Based on HRS IPD Technology. In Proceedings of the 2020 IEEE MTT-S International Microwave Workshop Series on Advanced Materials and Processes for RF and THz Applications (IMWS-AMP), Suzhou, China, 29–31 July 2020; pp. 1–3.
28. Lee, P.-N.; Hsieh, P.-C.; Hsieh, S.-C.; Kung, C.-Y.; Wang, C.-C. Design and Fabrication of Band-Pass Filter on Glass IPD for 5G New Radio. In Proceedings of the 2020 IEEE 70th Electronic Components and Technology Conference (ECTC), Orlando, FL, USA, 6 June 2020; pp. 1775–1780.
29. Dai, X.; Zhang, X.; Kao, H.-L.; Wei, B.-H.; Xu, J.-X.; Li, X. LTCC Bandpass Filter With Wide Stopband Based on Electric and Magnetic Coupling Cancellation. *IEEE Trans. Compon. Packag. Manuf. Technol.* **2014**, *4*, 1705–1713.
30. Zhu, Y.-Y.; Yang, Y.-J.; Chen, J.-X. High-performance bandpass filter using HTCC stepped-impedance resonators. *IET Microw. Antennas Propag.* **2018**, *12*, 56–62. [[CrossRef](#)]
31. Yang, Y.; Lu, R.; Gao, L.; Gong, S. 4.5 GHz Lithium Niobate MEMS Filters With 10% Fractional Bandwidth for 5G Front-Ends. *J. Microelectromechanical Syst.* **2019**, *28*, 575–577. [[CrossRef](#)]
32. Yang, Y.; Lu, R.; Gao, L.; Gong, S. A C-band Lithium Niobate MEMS Filter with 10% Fractional Bandwidth for 5G Front-ends. In Proceedings of the 2019 IEEE International Ultrasonics Symposium (IUS), Glasgow, UK, 6–9 October 2019; pp. 1981–1984.
33. Al-Yasir, Y.; Parchin, N.O.; Rachman, Z.-A.S.A.; Ullah, A.; Abd-Alhameed, R. Compact tunable microstrip filter with wide-stopband restriction and wide tuning range for 4G and 5G applications. In Proceedings of the IET's Antennas and Propagation Conference, Birmingham, UK, 11–12 November 2019; pp. 1–6.
34. Zuo, C.; He, C.; Cheng, W.; Wang, Z. Hybrid Filter Design for 5G using IPD and Acoustic Technologies. In Proceedings of the 2019 IEEE International Ultrasonics Symposium (IUS), Glasgow, UK, 6–9 October 2019; pp. 269–272.
35. Gao, L.; Yang, Y.; Gong, S. Wideband Hybrid Monolithic Lithium Niobate Acoustic Filter in the K-Band. *Ieee Trans. Ultrason. Ferroelectr. Freq. Control* **2020**. [[CrossRef](#)] [[PubMed](#)]
36. Al-Yasir, Y.I.A.; Parchin, N.O.; Alabdallah, A.; Abdulkhaleq, A.M.; Sajedin, M.; Elfergani, I.T.E.; Abd-Alhameed, R.A. Design, Simulation and Implementation of Very Compact Open-loop Trisection BPF for 5G Communications. In Proceedings of the 2019 IEEE 2nd 5G World Forum (5GWF), Dresden, Germany, 30 September–2 October 2019; pp. 189–193.
37. Kikkert, C.J. Designing Low Cost Wideband Microstrip Bandpass Filters. In Proceedings of the TENCON 2005–2005 IEEE Region 10 Conference, Melbourne, Australia, 21–24 November 2005; pp. 1–6.
38. Gupta, K.; Garg, R.; Bahl, I.; Bhartia, P. *Microstrip Lines and Slotlines*, 2nd ed.; Artech House: Boston, MA, USA, 1996.
39. Pozar, D. *Microwave Engineering*, 4th ed.; Wiley: Hoboken, NJ, USA, 2012.
40. Zhu, L.; Sun, S.; Menzel, W. Ultra-Wideband (UWB) Bandpass Filters Using Multiple-Mode Resonator. *IEEE Microw. Wirel. Compon. Lett.* **2005**, *15*, 796–798.
41. Sun, S.; Zhu, L. Capacitive-Ended Interdigital Coupled Lines for UWB Bandpass Filters With Improved Out-of-Band Performances. *IEEE Microw. Wirel. Compon. Lett.* **2006**, *16*, 440–442. [[CrossRef](#)]
42. Ren, B.; Liu, H.; Ma, Z.; Ohira, M.; Wen, P.; Wang, X. Compact Dual-Band Differential Bandpass Filter Using Quadruple-Mode Stepped-Impedance Square Ring Loaded Resonators. *IEEE Access* **2018**, *6*, 21850–21858. [[CrossRef](#)]
43. Ren, B.; Ma, Z.; Liu, H.; Guan, X.; Wen, P.; Ohira, M. Compact Multi-Band Differential Bandpass Filters Using Microstrip Multi-mode Resonators. In Proceedings of the IEEE MTT-S International Wireless Symposium (IWS), Guangzhou, China, 19–22 May 2019.
44. Alnahwi, F.; Islam, N. A Generalized Concept for Band Notch Generation in Ultra-Wide Band Antennas. *Prog. Electromagn. Res. C* **2014**, *54*, 179–185. [[CrossRef](#)]